

# Joint Reconstruction of Image and Motion in Gated Positron-Emission-Tomography

Moritz Blume, Axel Martinez-Möller, Andreas Keil, Nassir Navab and Magdalena Rafecas

**Abstract**—We present a novel method for joint reconstruction of both image and motion in positron-emission-tomography (PET). Most other methods separate image from motion estimation: They use deformable image registration/optical flow techniques in order to estimate the motion from individually reconstructed gates. Then, the image is estimated based on this motion information. With these methods, a main problem lies in the motion estimation step, which is based on the noisy gated frames. The more noise is present, the more inaccurate the image registration becomes.

As we show in a simulation study, our joint reconstruction approach overcomes these drawbacks and results in both visually and quantitatively better image quality. We attribute these results to the fact that for motion estimation always the currently best available image estimate is used and vice versa. Additionally, results for real dual respiratory and cardiac gated patient data are presented.

**Index Terms**—PET, reconstruction, motion compensation, gating.

## I. INTRODUCTION

With increasing physical resolution of nowadays positron-emission-tomography (PET) scanners, even small patient motion can significantly reduce the image quality and thus lead to false diagnosis. The goal of motion compensation methods in PET is to reconstruct the image as if no motion had taken place.

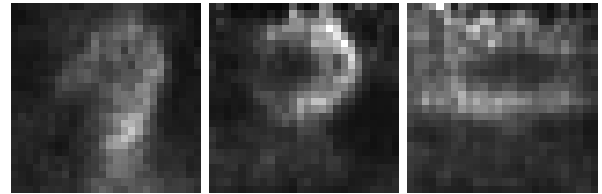
Most of current motion compensation methods consist of two steps: (i) motion estimation and (ii) image estimation.

A popular way to estimate respiratory and/or cardiac motion is to (a) divide the measured data into different gates according to the cardiac/respiratory cycle, (b) reconstruct each gate by a state-of-the-art PET reconstruction method (such as maximum-likelihood expectation-maximization, ML-EM, [1]) and (c) register each frame to a reference frame. For gated PET, this has been done with affine motion models [2], non-rigid b-spline models [3] and optical flow [4]–[7].

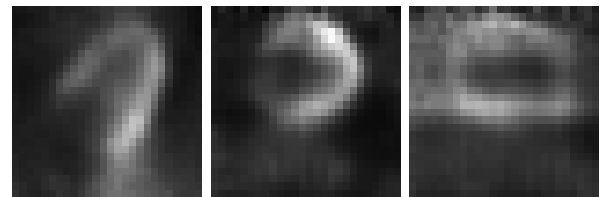
In the second step, the image is estimated based on the available knowledge about motion. A very common approach is to deform reconstructed gates to the reference frame and then combine them (usually by taking the sum of these

M. Blume is affiliated to both the Instituto de Física Corpuscular (IFIC), Universidad de Valencia / CSIC, Valencia, Spain and Computer Aided Medical Procedures (CAMP), Department of Computer Science, Technische Universität München, Munich, Germany. M. Rafecas is with the IFIC. A. Keil and N. Navab are with CAMP. A. Martinez-Möller is affiliated to both CAMP and the Nuklearmedizinische Klinik im Klinikum Rechts der Isar, Technische Universität München, Munich, Germany.

Author contact: Moritz Blume, IFIC - Instituto de Física Corpuscular, Edificio Institutos de Investigación, Apartado de Correos 22085, E-46071 Valencia - Spain; Phone: +34963543237; E-Mail: moritz.blume@cs.tum.edu



(a) Reconstruction of one gate with ML-EM



(b) Reconstruction of the same gate with our proposed joint reconstruction method

Fig. 1: Transverse, coronal and sagittal views of a human's heart for a real 10 minutes  $^{18}\text{F}$ FDG PET scan.

deformed frames) [4]–[7]. More sophisticated methods use an adapted ML-EM algorithm which is able to deal with arbitrary non-rigid motion [3], [8], [9].

A major drawback of these methods lies in the motion estimation step. On the one hand, one wants to have as many gates as possible in order to accurately measure the motion. On the other hand, using more gates implies less photon counts in each gate and thus leads to noisier reconstructed images on which the motion estimation is based. So, with an increasing number of gates, the motion estimation step becomes more and more likely to be of low accuracy or even fail completely.

Beyond the described methods which separate motion estimation from image estimation, another (much smaller) class of algorithms that jointly estimates image and motion has emerged. It can be broadly sub-classified into two categories: those that use a different image estimate for each frame [10]–[12], and those that use a common image estimate for all frames [13].

In this work, we present a novel method for joint estimation of image and motion. We use a common image estimate and - in contrast to [13] - a deformable motion model. Our method uses all available counts and thus leads to reconstructions which are much less noisy (see Figure 1b). It is possible to visualize the motion instances for every gate.

## II. MATERIALS AND METHODS

### A. Joint Reconstruction

In the following, we describe a mathematical model for gated image acquisition in PET. Based on this model we develop a cost functional for reconstruction which depends on both image and motion and is subject to minimization.

1) *Model*: It is well known that, ideally, the relationship between an image  $f : \mathbb{R}^3 \mapsto \mathbb{R}$  and measurement data  $\hat{g} : \mathbb{N} \mapsto \mathbb{R}$  in PET can be modeled as  $\hat{g}(a) = \int H(a, \mathbf{x})f(\mathbf{x}) d\mathbf{x}$ .  $H : \mathbb{N} \times \mathbb{R}^3 \mapsto \mathbb{R}$  is the system model which contains the probability that the two annihilation photons emitted at position  $\mathbf{x}$  will be measured in line-of-response (LOR)  $a$ .

We extend this model to

$$\sum_t \hat{g}(a, t) = \frac{1}{T} \sum_t \int H(a, \mathbf{x})f(\varphi(\mathbf{x}, t)) d\mathbf{x} \quad (1)$$

in the case of subject motion. Here,  $T$  is the number of gates and  $\varphi(\mathbf{x}, t) : \mathbb{R}^3 \times \mathbb{N} \mapsto \mathbb{R}^3$  represents the deformation field of image  $f$  at gate  $t$  with respect to an arbitrary reference gate  $t_{\text{ref}}$  (this implies  $\varphi(\mathbf{x}, t_{\text{ref}}) = \mathbf{x}$ ).

2) *Cost Functional*: Our preliminary goal is to build a cost functional  $\mathcal{D}(f, \varphi)$  in such manner that a tuple of image  $f^*$  and  $\varphi^*$  for which  $\mathcal{D}(f^*, \varphi^*)$  is minimal fits to the above model as well as possible. Then, we introduce a regularization term in order to encourage physically meaningful deformation fields.

a) *Dissimilarity Term*: It is well known that the number of counts  $g(a, t)$  that is measured for an LOR  $a$  is distributed by a Poisson random variable:

$$P(g(a, t)|f, \varphi) = e^{-\hat{g}(a, t)} \cdot \frac{\hat{g}(a, t)^{g(a, t)}}{g(a, t)!}, \quad (2)$$

where  $\hat{g}(a, t) = \frac{1}{T} \int H(a, \mathbf{x})f(\varphi(\mathbf{x}, t)) d\mathbf{x}$  is the estimated measurement vector given an image  $f$  and transformation  $\varphi$ .

The likelihood function for all measured events of a gate  $t$  is

$$L(f, \varphi|g(a, t)) = \prod_a P(g(a, t)|f, \varphi). \quad (3)$$

We seek to find a pair of image  $f$  and motion  $\varphi$  that maximizes the likelihood function for all gates. This is equivalent to minimizing the negative log-likelihood function

$$\log(-L(f, \varphi)) = \sum_t \sum_a \hat{g}(a, t) - g(a, t) \log(\hat{g}(a, t)) + \log(g(a, t)!). \quad (4)$$

Here,  $\sum_t \sum_a \log(g(a, t)!)$  can be omitted since it does not affect the minimum. So, finally we arrive at

$$\mathcal{D}(f, \varphi) = \sum_t \sum_a \hat{g}(a, t) - g(a, t) \log(\hat{g}(a, t)) \quad (5)$$

which is subject to minimization.

b) *Regularization*: In order to prohibit extreme deformations we use homogeneous diffusion regularization, which is well known in the image registration community:

$$\mathcal{S}(\varphi) = \sum_t \sum_{i=1}^3 \int \|\nabla_{\mathbf{x}} \varphi_i(\mathbf{x}, t)\|^2 d\mathbf{x} \quad (6)$$

We initially also employed smoothing in the time domain, however, no differences in the reconstruction could be noted.

Finally, the complete cost functional we seek to minimize is

$$\mathcal{J}(f, \varphi) = \mathcal{D}(f, \varphi) + \alpha \mathcal{S}(\varphi). \quad (7)$$

The regularization parameter  $\alpha$  defines the smoothness of our sought deformation. It has to be carefully adjusted to the specific case. If it is too high the resulting  $\varphi$  will represent no visible deformation and thus the resulting image  $f$  will still suffer from motion blur. Is it too low,  $\mathcal{J}$  will be over-fitted and an unrealistic pair of image and motion results. Section III contains more information on the right choice of  $\alpha$ .

### B. Registration and Fusion of Reconstructed Frames (RFRF)

We choose the RFRF approach for comparison since it is a common motion compensation method in cardiac PET. It can be separated in the motion estimation and the image estimation step.

Motion estimation: we register each of the already reconstructed gates to a reference gate (in this case the first gate). Registration is done by an optimization approach where we seek to optimize the following cost functional:

$$\mathcal{R}(\varphi_{\text{RFRF}}) = \sum_t \int (f_t(\mathbf{x}) - f_0(\varphi_{\text{RFRF}}(\mathbf{x}, t)))^2 d\mathbf{x} + \alpha \mathcal{S}(\varphi_{\text{RFRF}}). \quad (8)$$

$f_t$  is pre-reconstructed  $t$ -th gate.  $\varphi_{\text{RFRF}}$  is the sought time-dependant transformation field that transforms  $f_0$  to the respective gate.  $\mathcal{S}$  is the homogeneous diffusion regularization term from equation (6). Note that for the first gate we get the identity transformation:  $\varphi_{\text{RFRF}}(\mathbf{x}, 0) = \mathbf{x}$ .

The image estimation is a summation of the transformed gates:  $f_{\text{RFRF}}(\mathbf{x}) = \sum_t f_t(\varphi_{\text{RFRF}}^{-1}(\mathbf{x}, t))$ .

### C. Data

We test our algorithm for both simulated and real data.

1) *Simulation*: We generate 32 frames using the XCAT phantom [14]. One complete respiratory cycle of a length of five seconds is simulated, without any cardiac motion. The extent of diaphragm motion is set to two centimeters. These 32 frames are then redistributed to eight gates. In doing so we make sure that motion is simulated also within a gate. For each gate, a volume of  $50 \times 50 \times 50$  voxels containing the heart is cropped.

The expected number of counts for each LOR is calculated by projecting each gate to measurement space. The measurements are finally generated from the expected number

of counts by a Poisson random generator. This way we take into account the acquisition time and activity. Ten levels of statistical noise, representing very long to extremely short acquisition times, were simulated.

Since we want to focus on image degradations induced by motion, we did not make use of external simulation packages which would include effects like scattering, random coincidences etc. We simulate a Siemens Biograph Sensation 16 PET/CT scanner and use Scheins’s algorithm to generate the system matrix [15].

2) *Real Data*: The patient data was taken from a previously accomplished cardiac examination which measured the myocardial metabolism in order to assess tissue viability. It was acquired with a Siemens Biograph Sensation 16 PET/CT scanner. The injected dose of  $^{18}\text{F}$ -FDG was roughly 400 MBq. The patient had to rest for 60 minutes before data acquisition started. Both the respiratory and the ECG signal were recorded and later used in order to divide the data into eight respiratory gates by omitting the systolic phase and combining all diastolic phases into one (since the diastolic phase is the longest cardiac phase with minimal motion).

As for the simulation, we also use Scheins’s algorithm for calculating the system matrix. Due to memory and computational complexity we have to use an adaptive voxel grid: within a predefined region-of-interest (ROI) the grid is constant and fine ( $0.4 \times 0.4 \times 0.4 \text{ mm}^3$ ) and outside the ROI it gets exponentially coarser.

#### D. Data Analysis

For the simulated data, we compare our joint reconstruction approach (JR) to an ML-EM reconstruction (30 iterations) for motion-contaminated data (MC), an ML-EM reconstruction (30 iterations) for the first gate (FG), the RFRF approach (as described in section II-B) and an ML-EM reconstruction (30 iterations) for motion-free data (MF).

As reference frame for all comparisons we choose the first gate. In case of our joint reconstruction approach, we map the resulting image  $f$  to the first gate by applying the reconstructed deformation  $\varphi$ :  $f(\varphi(\mathbf{x}, t))$ .

As a quantitative measure for evaluation we use the correlation coefficient  $CC(\mathbf{x}, \mathbf{y}) = \frac{\mathbf{x}^T \mathbf{y}}{\|\mathbf{x}\| \|\mathbf{y}\|}$  between the reconstructed image of the respective reconstruction approach (represented by a vector  $\mathbf{x}$ ) and the original image (represented by a vector  $\mathbf{y}$ ). Both  $\mathbf{x}$  and  $\mathbf{y}$  are shifted such that their mean value is zero.

In addition, we provide selected resulting images for visual inspection. For real data, no quantitative analysis is possible and one has to rely on visual inspection.

### III. RESULTS AND DISCUSSION

#### A. Simulation

Table I summarizes the results for different noise levels. Figure 2 shows visually selected transverse, coronal and sagittal slices for three levels of noise. The level of noise is indicated by the number of annihilation events - the less events, the higher the level of noise.

Counts	MC	FG	RFRF	JR	MF
9.00e+07	0.93	0.98	0.97	0.99	0.99
4.50e+07	0.93	0.97	0.97	0.98	0.99
2.25e+07	0.93	0.95	0.96	0.98	0.99
1.13e+07	0.92	0.91	0.94	0.98	0.98
5.60e+06	0.91	0.85	0.89	0.97	0.97
2.80e+06	0.88	0.74	0.77	0.96	0.95
1.40e+06	0.84	0.62	0.61	0.93	0.91
7.00e+05	0.76	0.48	0.46	0.87	0.85
3.50e+05	0.65	0.36	0.33	0.78	0.74

TABLE I: Simulation: quantitative evaluation for different reconstruction scenarios. We calculate the correlation coefficient of the respective reconstruction method and the original image. We compare an ML-EM reconstruction of the motion-contaminated data (MC), an ML-EM reconstruction of just the first gate (FG), the registration and fusion of reconstructed frames (RFRF) as described in the methods section, our joint reconstruction (JR) and an ML-EM reconstruction of motion-free data (MF).

JR performs better than MC, FR and RFRF in all cases. Especially for moderate and high noise levels the difference is striking.

Comparing JR to MF, it is surprising that JR has an even higher correlation coefficient for high noise levels. Consulting Figure 2c reveals that this observation may be attributed to the fact that the joint reconstruction is less noisy than the reconstruction for motion-free data.

Interestingly, RFRF works better than MC only for low and moderate noise levels. Our explanation is two-fold: firstly, image registration in the RFRF approach becomes more and more inaccurate with increasing noise. Secondly, fusion by summation *in image space* is a permissible approximation only for low-noise scenarios.

#### B. Real Data

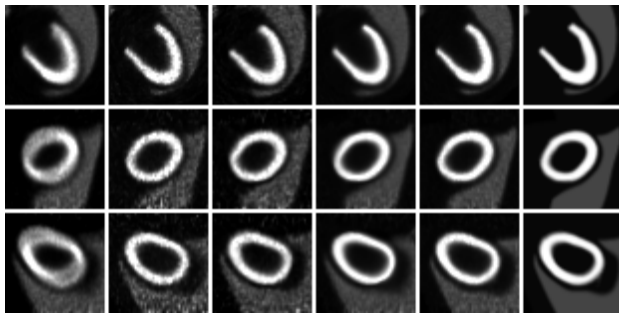
Figure 3 compares our JR approach (fourth column) to MC, FG and RFRF. It clearly shows the better defined myocardial walls, indicating the potential to achieve a notable reduction of the motion induced blur.

### IV. CONCLUSION

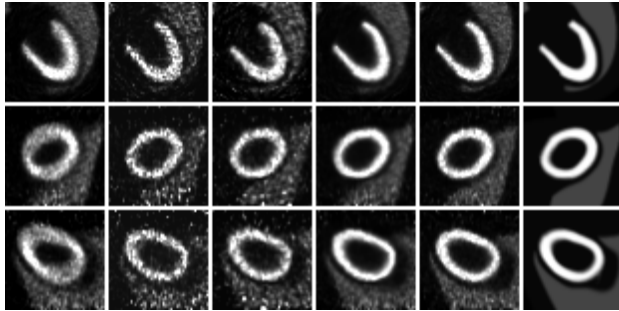
We present a novel motion compensation algorithm for gated positron-emission-tomography. Our method jointly reconstructs both image and motion. We compare our method to a registration-and-fusion-of-reconstructed-frames approach which is a typical ambassador of methods that separate image from motion estimation. In a simulation study, both quantitative and visual comparison clearly proof the superior reconstruction quality of our method for all simulated noise conditions, particularly in high noise scenarios. The paper concludes with results for real dual respiratory and cardiac gated patient data which further underline its potential in reducing motion blur.

#### REFERENCES

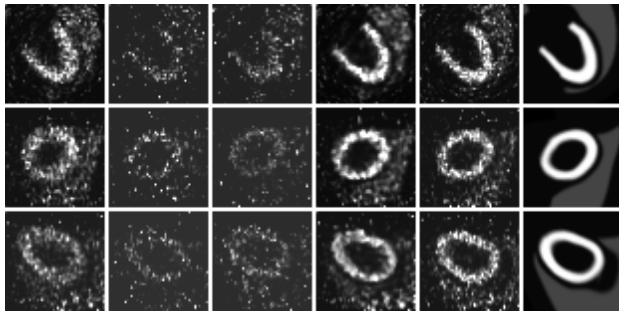
- [1] L. A. Shepp and Y. Vardi, “Maximum likelihood reconstruction for emission tomography,” *Image Processing, IEEE Transactions on*, vol. 1, no. 2, pp. 113–122, 1982.



(a) Moderate noise:  $9.00e+07$  annihilation events



(b) High noise:  $1.13e+07$  annihilation events



(c) Extremely high noise:  $7.00e+05$  annihilation events

Fig. 2: Selected transverse, coronal and sagittal slices for different levels of noise and different reconstruction scenarios for the simulated data (from left to right): ML-EM reconstruction of motion-contaminated data (MC), ML-EM reconstruction of just the first gate (FG), registration and fusion of reconstructed frames (RFRF, as described in section II-B), our joint reconstruction (JR) and ML-EM reconstruction of motion-free data (MF). For comparison, the original image is shown in the last column.

- [2] F. Lamare, T. Cresson, J. Savean, C. C. L. Rest, A. J. Reader, and D. Visvikis, "Respiratory motion correction for PET oncology applications using affine transformation of list mode data," *Physics in Medicine and Biology*, vol. 52, no. 1, pp. 121–140, 2007. [Online]. Available: <http://stacks.iop.org/0031-9155/52/121>
- [3] F. Lamare, M. J. L. Carbayo, T. Cresson, G. Kontaxakis, A. Santos, C. Cheze, L. Rest, A. J. Reader, and D. Visvikis, "List-mode-based reconstruction for respiratory motion correction in PET using non-rigid body transformations," *Physics in Medicine and Biology*, vol. 52, no. 17, pp. 5187–, 2007.
- [4] G. J. Klein, B. W. Reutter, and R. H. Huesman, "Non-rigid summing of gated PET via optical flow," in *Nuclear Science Symposium, 1996. Conference Record., 1996 IEEE*, vol. 2, Anaheim, CA, USA, Nov. 1996, pp. 1339–1342.
- [5] G. J. Klein, "Four-dimensional processing of deformable cardiac PET data," in *Mathematical Methods in Biomedical Image Analysis, 2000. Proceedings. IEEE Workshop on*, Hilton Head Island, SC, USA, 2000,

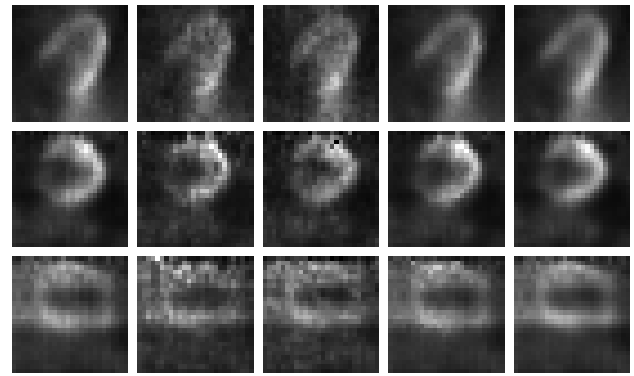


Fig. 3: Transverse, coronal and sagittal slices for real patient data (from left to right): ML-EM reconstruction of motion-contaminated data (MC), ML-EM reconstruction of just the first gate (FG), registration and fusion of reconstructed frames (RFRF, as described in section II-B) and our joint reconstruction (JR).

- pp. 127–134.
- [6] G. J. Klein, B. W. Reutter, and R. H. Huesman, "4d affine registration models for respiratory-gated PET," in *Nuclear Science Symposium Conference Record, 2000 IEEE*, vol. 2, Lyon, France, 2000, pp. 41–15.
- [7] M. Dawood, N. Lang, X. Jiang, and K. P. Schäfers, "Lung motion correction on respiratory gated 3-D PET/CT images," *IEEE Transactions on Medical Imaging*, vol. 25, no. 4, pp. 476–485, Apr. 2006.
- [8] F. Qiao, T. Pan, J. W. C. Jr, and O. R. Mawlawi, "A motion-incorporated reconstruction method for gated pet studies," *Physics in Medicine and Biology*, vol. 51, no. 15, pp. 3769–3783, 2006. [Online]. Available: <http://stacks.iop.org/0031-9155/51/3769>
- [9] M. Reyes, G. Malandain, P. M. Koulibaly, M. A. González-Ballester, and J. Darcourt, "Model-based respiratory motion compensation for emission tomography image reconstruction," *Physics in Medicine and Biology*, vol. 52, no. 12, pp. 3579–3600, 2007. [Online]. Available: <http://stacks.iop.org/0031-9155/52/3579>
- [10] B. Mair, D. Gilland, and J. Sun, "Estimation of images and nonrigid deformations in gated emission ct," *IEEE transactions on Medical Imaging*, vol. 25, no. 9, pp. 1130–1144, Sept. 2006.
- [11] E. Gravier, Y. Yang, M. A. King, and M. Jin, "Fully 4d motion-compensated reconstruction of cardiac spect images this work was supported in part by the national institutes of health under grant no hl65425." *Physics in Medicine and Biology*, vol. 51, no. 18, pp. 4603–4619, 2006. [Online]. Available: <http://stacks.iop.org/0031-9155/51/4603>
- [12] J. Parker and D. Gilland, "Wall motion estimation for gated cardiac emission tomography: Physical phantom evaluation," *IEEE transactions on Nuclear Science*, vol. 55, no. 1, pp. 531–536, Feb. 2008.
- [13] H. Schumacher, J. Modersitzki, and B. Fischer, "Combined reconstruction and motion correction in SPECT imaging," *IEEE transactions on Nuclear Science*, vol. 56, pp. 73–80, 2009.
- [14] W. P. Segars, "Development and application of the new dynamic nurbs-based cardiac-torso (ncat) phantom," Ph.D. dissertation, University of North Carolina, 2001.
- [15] J. J. Scheins, F. Boschen, and H. Herzog, "Analytical calculation of volumes-of-intersection for iterative, fully 3-d PET reconstruction," *IEEE Transactions on Medical Imaging*, vol. 25, no. 10, pp. 1363–1369, Oct. 2006.